Ab initio analysis of nucleation reactions during tungsten atomic layer deposition on Si(100) and W(110) substrates

Mariah J. King, Patrick L. Theofanis, Paul C. Lemaire, Erik E. Santiso, and Gregory N. Parsons

Citation: Journal of Vacuum Science & Technology A 36, 061507 (2018); doi: 10.1116/1.5044740

View online: https://doi.org/10.1116/1.5044740

View Table of Contents: https://avs.scitation.org/toc/jva/36/6

Published by the American Vacuum Society

ARTICLES YOU MAY BE INTERESTED IN

Rapid atomic layer etching of Al₂O₃ using sequential exposures of hydrogen fluoride and trimethylaluminum with no purging

Journal of Vacuum Science & Technology A 36, 061508 (2018); https://doi.org/10.1116/1.5043488

Thermal atomic layer etching of HfO₂ using HF for fluorination and TiCl₄ for ligand-exchange Journal of Vacuum Science & Technology A **36**, 061504 (2018); https://doi.org/10.1116/1.5045130

Review Article: Atomic layer deposition for oxide semiconductor thin film transistors: Advances in research and development

Journal of Vacuum Science & Technology A 36, 060801 (2018); https://doi.org/10.1116/1.5047237

Thermal atomic layer deposition of Sn metal using SnCl₄ and a vapor phase silyl dihydropyrazine reducing agent Journal of Vacuum Science & Technology A **36**, 06A106 (2018); https://doi.org/10.1116/1.5055212

Atomic layer deposition of Al₂O₃ and TiO₂ on MoS₂ surfaces

Journal of Vacuum Science & Technology A 36, 06A101 (2018); https://doi.org/10.1116/1.5043621

Overview of atomic layer etching in the semiconductor industry

Journal of Vacuum Science & Technology A 33, 020802 (2015); https://doi.org/10.1116/1.4913379





Ab initio analysis of nucleation reactions during tungsten atomic layer deposition on Si(100) and W(110) substrates

Mariah J. King,¹ Patrick L. Theofanis,² Paul C. Lemaire,¹ Erik E. Santiso,¹ and Gregory N. Parsons^{1,a)}

(Received 15 June 2018; accepted 12 September 2018; published 8 October 2018)

Novel insight into the mechanisms that govern nucleation during tungsten atomic layer deposition is presented through a detailed analysis using density functional theory. Using the calculated energetics, the authors suggest the most probable series of reactions that lead to monolayer formation on desired growth surfaces, Si(100) and W(110), during sequential doses of WF₆ and SiH₄. From this analysis, they conclude that a relatively high-energy barrier exists for initial nucleation of WF₆ on a silicon substrate; therefore, the system is limited to physical adsorption and is only capable of accessing nucleation pathways once the reaction barrier is energetically accessible. During early doses of WF₆, the initial silicon surface acts as the reductant. Results from this half-reaction provide support for the noncoalesced growth of initial W layers since nucleation is shown to require a 2:1 ratio of silicon to WF₆. In addition, the release of H₂ is significantly favored over HF production leading to the formation of fluorine-contaminated silicon sites; etching of these sites is heavily supported by the absence of fluorine observed in experimentally deposited films as well as the high volatility of silicon-subfluorides. In the second half-reaction, SiH₄ plays the multipurpose role of stripping fluorine atoms from W, displacing any adsorbed hydrogen atoms, and depositing a silicon-hydride layer. Saturation of the previously formed W layer with silicon-hydrides is a crucial step in depositing the consecutive layer since these surface species act as the reductants in the succeeding dose of WF₆. The SiH₄ halfreaction reaches a limit when all fluorine atoms are removed as silicon-subfluorides (SiF_xH_y) and tungsten sites are terminated with silicon-hydrides. The WF₆ dose reaches a limit in early doses when the reductant, i.e., the surface, becomes blocked due to the formation of a planar network of fluorine-containing tungsten intermediates and in later cycles when the reductant, i.e., adsorbed silicon-hydrides, is etched entirely from the surface. Overall, the calculated energetics indicate that WF_xH_y , SiF_x , and H_2 molecules are the most probable by-products released during the ALD process. Results from this work contribute significantly to the fundamental understanding of atomic layer growth of tungsten using silicon species as reducing agents and may be used as a template for analyzing novel ALD processes. Published by the AVS. https://doi.org/10.1116/1.5044740

I. INTRODUCTION

The semiconductor industry is actively focused on developing atomic layer deposition (ALD) techniques for insulating, semiconducting, and conducting materials that allow for atomically thin device layers with defect-free film composition. Using ALD, single atomic layers can be deposited allowing for enhanced control of thin film growth and a means by which to reduce the restrictive 7-nanometer node size available to the industry. Well-established ALD processes exist for specific chemical systems and are currently employed in the semiconductor industry for the deposition of metal thin films for source and drain contacts, gate dielectrics, and in the deposition of seed layers for Damascene metal deposition in interconnects and vias.^{2,3} However, the potential for ALD application remains abundant and is contingent on increasing the accuracy of existing half-reactions and development of novel processes. Using existing ALD half-reactions, atomistic studies can be used to thoroughly understand self-limiting mechanisms in order to increase the accuracy of current processes and create a template by which to design new processes for desirable materials.

Tungsten ALD (W-ALD) is an example of a wellestablished process that is currently employed in the semiconductor industry. Deposition of W via silane reduction was first confirmed in 1987 at a high deposition rate in a low-temperature range,⁴ and after nearly two decades of extensive research on W chemical vapor deposition, George et al. demonstrated deposition of W using sequential doses of WF₆ and Si₂H₆.⁵ Their successful validation of selflimiting surface reactions led to a new ALD process for tungsten that offered enhanced control of composition, thickness, and conformality.^{5,6} Tungsten is a highly desirable material for its properties, such as resistance to high temperatures, hardness, high thermal and conductive properties, and chemical inertness to oxidation, so the ALD process is widely used in contact and diffusion barriers, low resistance gates and interconnect lines in a VLSI circuit and continues to be developed for applications in Area-Selective ALD and as a template for novel chemistries.^{7–9}

¹Department of Chemical and Biomolecular Engineering, North Carolina State University, Raleigh, North Carolina 27695

²Intel Corporation, 2501 NE Century Blvd., Hillsboro, Oregon 97124

a)Electronic mail: gnp@ncsu.edu

The most common tungsten ALD and CVD processes use tungsten hexafluoride, which can be reduced by silane, hydrogen, or crystalline silicon surface sites, with silane and crystalline silicon being the most commonly used due to their high-rate, low-temperature process conditions. Despite the numerous studies on tungsten ALD/CVD, the physiochemical characteristics that control tungsten growth have yet to be sufficiently described and the chemical pathways that drive deposition remain contested; an example being the disputed emission of HF and tungsten subfluorides. 10-12 In addition, the self-limiting half-reactions are often described using a single reaction mechanism with unspecified stoichiometry, while in reality the half-cycles proceed through a series of unidentified subreactions. Furthermore, deposited thin films have a high surface-to-volume ratio making an atomistic understanding of surface chemistries crucial in increasing the accuracy and efficiency of the existing process.

In this paper, we present an *ab initio* analysis of the W-ALD process in order to enhance the understanding of a nucleation phenomenon and provide a unique perspective into the specific chemistries that influence monolayer growth. Using density functional theory (DFT), we perform a systematic exploration of potential reaction pathways to identify the most probable reactions that lead to nucleation during the W-ALD self-limiting half-reactions. DFT is a standard quantum mechanical method that is often applied to systems involving metallic and semiconducting materials¹³ in which experimental studies, such as W-ALD, are limited by inconsistent results and nonequilibrium conditions. This study focuses specifically on W-ALD using WF₆ and SiH₄ as precursors and selectively terminated Si(100) and W(110) as substrate surfaces.

This work is organized as follows: the Methods section provides DFT and reaction pathway calculation parameters as well as the method used to generate geometry files; the Results and Discussion sections are organized sequentially according to the corresponding half-cycle. The Results section provides details on identified reaction mechanisms, and the Discussion section provides an analysis of the results in light of experimental evidence.

II. SIMULATION METHODS

We performed calculations using the *ab initio* plane-wave pseudopotential approach as implemented in the Vienna *Ab initio* Simulation Package. ^{17,18} The Perdew–Wang (PW91) functional was used to perform periodic DFT calculations with valence electrons treated explicitly. Interactions within the ionic cores were described using the projector augmented-wave method, which allowed for an energy cutoff of 400 eV to be specified. The gamma point was used in the Brillouin-zone integration with a $6 \times 6 \times 1$ k-point mesh, and the positions of all atoms were relaxed self-consistently until the total energy difference decreased below 10^{-4} eV.

Hydrated silicon [Si(100)-H] and fluorinated-tungsten [W(110)-F] slabs were used to imitate surfaces available during tungsten ALD. To prepare the slabs, the unit cells of the substrate were allowed to relax in volume, shape, and atomic coordinates. The unit cell was then replicated and cleaved along a

given Miller plane and vacuum was added above and below the slab to create a semiperiodic simulation. The midsection atoms were frozen to approximate the bulk substrate and, in some cases, the surface atoms were passivated to eliminate dangling electrons. Finally, surfaces were relaxed into their ground state.

Interaction energies were calculated for surface interactions using the general equation:

$$\Delta E_{0,Interaction} = [E_{(0,Slab)} + E_{(0,Precursor)}] - [E_{(0,Slab+Adsorbant}) + E_{(0,by-products)}].$$
(1)

The reaction mechanisms and rates were calculated using the zero-temperature string method (ZTSM). This method is an interpolation algorithm that requires both reactant and product configurations to generate a sequence of configurations along the reaction coordinate. 19,20 The coordinates of the generated configurations are connected by a "string" that is optimized during the reparametrization step in the direction of the force normal to the string. The sequence of configurations is then regenerated along the optimized string. The bulk of computational time required is due to the cost associated with calculating forces on each atom in the system, which are used during the reparametrization step. This cost can be reduced by "freezing" bulk atoms in the slab. One particular advantage of ZTSM is the ability to choose the parametrization density, or the spacing of configurations on the reaction coordinate, based on intrinsic properties that are relevant to the system at hand. In this particular study, we used two reparametrization conditions in order to develop a more descriptive representation of the reaction pathway: an equal spacing and energy-weighted spacing of the configurations (Fig. 1).

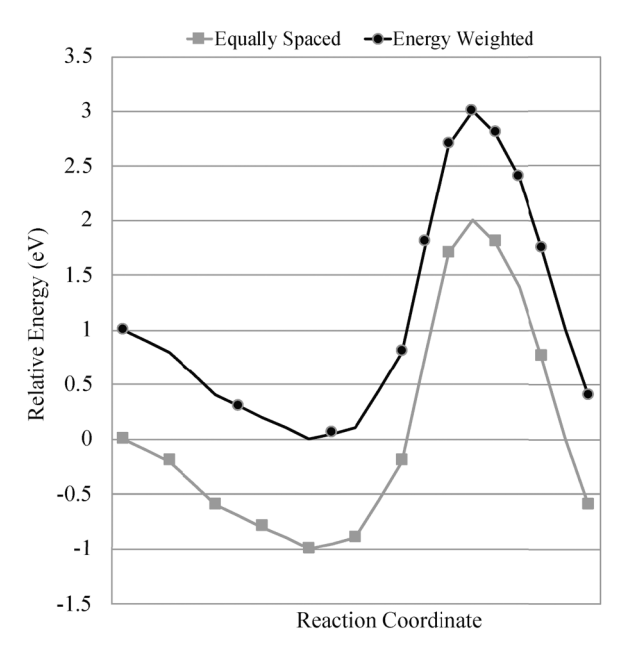


Fig. 1. Illustration of image spacing options along the reaction coordinate during the reparametrization step of the zero-temperature string method: energy-weighted spacing of configurations and equal spacing of configurations.

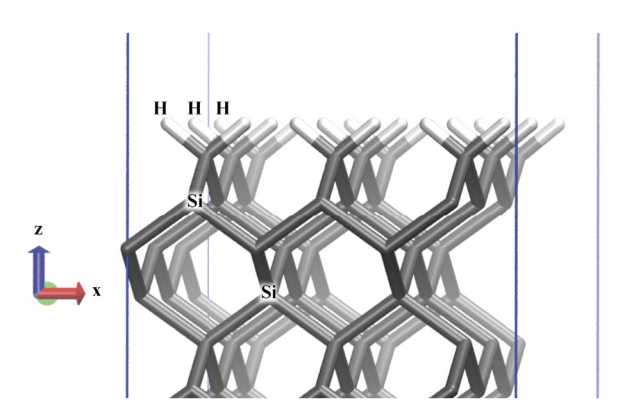


Fig. 2. Top half of a seven-layer silicon slab with 100 orientation and hydrogen passivation: silicon atoms (dark grey) and hydrogen atoms (white). Periodic boundary conditions were employed to approximate the bulk substrate.

The reaction path was divided into 12–15 configurations, depending on the complexity of the reaction. The "time-step" for numerical integration of the equation of motion during the reparametrization step was chosen so that the maximum change in atom position was 0.05 Å.

A. Surface model descriptions

Adsorption was performed on the (100) plane of silicon A4 diamond since it is known to have the lowest surface energy (1.28 eV/Ų) and the semiconductor industry typically works on this surface. The supercell dimensions for the silicon substrate were $11.57\text{Å} \times 11.57\text{Å} \times 19.12\text{Å}$, which was equivalent to $3 \times 3 \times 5$ unit cells. The substrate contained a slab of 12 layers thick with 108 silicon atoms and 36 surface hydrogen atoms and the system contained the equivalent of two unit cells (7.72 Å) of vacuum. The top half of the hydrogenterminated silicon (100) surface is represented in Fig. 2.

Tungsten was modeled as a body-centered cubic lattice using a supercell with dimensions of 9.51 Å × 13.45 Å × 17.71 Å ×, which was equivalent to $3 \times 4 \times 5$ unit cells. The substrate contained a slab of 7 layers with 63 tungsten atoms and 18 surface fluorine atoms with the equivalent of 3.5 unit cells (11.06 Å) of vacuum. Adsorption was performed on the W(110) surface since this surface was identified by Jain *et al.* to have the lowest surface energy versus W(111) and W(100). The top half of the fluorine-terminated tungsten surface is represented in Fig. 3.

III. RESULTS

The standard W-ALD process proceeds through the following steps: WF $_6$ is exposed to hydrogen-terminated silicon with 100 orientation to produce surface tungsten fluorides; the system is purged to remove unused reactants and gaseous by-products; SiH $_4$ is exposed to the tungsten fluoride surface to produce silicon-hydrides, analogous to the starting Si-H surface; the system is purged to remove by-products. These steps, illustrated in Fig. 4, result in tungsten growth and are repeated until desired film thickness is achieved.

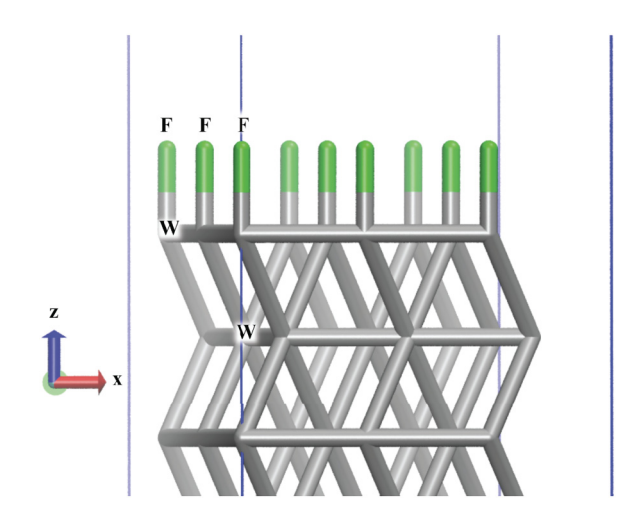


Fig. 3. Top half of tungsten slab with 110 orientation and fluorine passivation. Periodic boundary conditions were employed to appromixate the bulk substrate. Periodic boundary conditions were employed to approximate the bulk substrate.

A. Nucleation of WF₆ on hydrogen-terminated Si(100)

During the initial dose of WF_6 onto a hydrogenterminated silicon [Si(100)-H], the overall, unbalanced reaction can be expressed as follows:

$$Si(100) - H_{(s)} + WF_{6,(g)} \rightarrow Si(100) - WF_aH_{b,(s)} + SiF_xH_{v,(g)} + H_{2,(g)}/HF_{(g)}.$$
(2)

In reality, the above reaction proceeds through an unidentified number of subreactions. Using elementary reaction steps, we identify these subreactions, as well as intermediate species that exist during nucleation on Si(100). The identified species and calculated energy differences for each elementary step are shown in the overall schematic in Fig. 5. This reaction cascade, detailed through this section, illustrates the pathways identified as thermodynamically probable, indicated by straight, downward paths, and less probable, indicated by outward reaction paths.

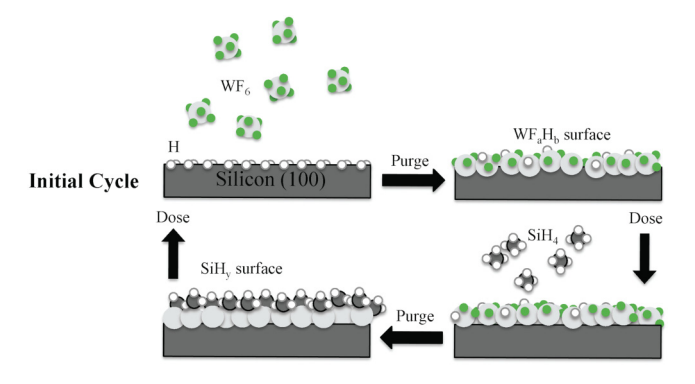


Fig. 4. Schematic of W-ALD: the top half depicts tungsten hexafluoride molecules being exposed to a silicon slab and the bottom half depicts silane molecules being exposed to a WFxHy-terminated silicon slab.

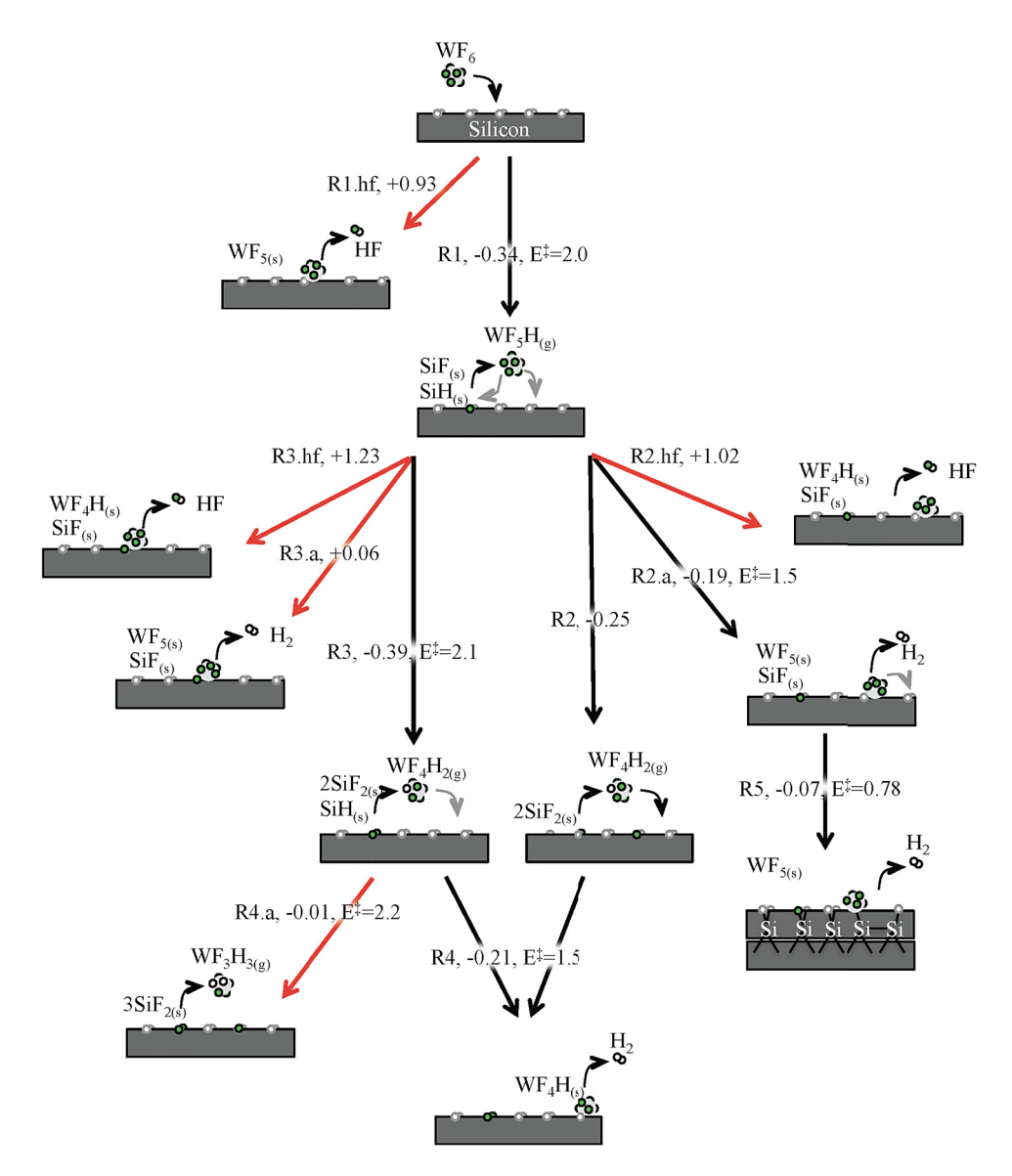


Fig. 5. Reaction scheme of WF₆ and hydrogen-passivated silicon surface with 100 orientation leading to the production of HF, H_2 , WF_aH_b , and chemisorbed W species. All energy values are given in units of electron volts (eV).

As depicted in the first step in Fig. 5, upon the introduction of WF_6 to hydrogen-terminated silicon (100), two elementary reactions are available to the system. These reaction mechanisms along with corresponding energy differences and activation barriers are presented in Eqs. (R1) and (R1.hf). Reaction labels including "hf," i.e., (R1.hf), denote alternate reaction paths that result in HF production, while those including "a" denote an alternate path for the same reactants

$$\begin{split} H-Si(100)-H+WF_{6,(g)} &\to H-Si(100)-F+WF_5H_{(g)},\\ \Delta E=-0.34\,\text{eV},\ E_{\frac{1}{4}}=2.01\,\text{eV}, \end{split}$$
 (R1)

$$\begin{aligned} &H-\text{Si}(100)-\text{H}+\text{WF}_{6,(g)}\rightarrow H-\text{Si}(100)-\text{WF}_5+\text{HF}_{(g)},\\ &\Delta E=+0.93\,\text{eV},\ E_{\frac{1}{4}}=2.76\,\text{eV}, \end{aligned} \tag{R1.hf}$$

where the given energy values are in eV. For both pathways, WF₆ physisorbs onto the surface with a binding energy of $-0.52 \,\mathrm{eV}$. From this state, the ligand exchange reaction, forming WF₅H (R1), is exothermic ($\Delta E = -0.34 \,\mathrm{eV}$) with a barrier (E_{\uparrow}) of 2.01 eV and is therefore more favorable than the reaction producing HF (R1.hf) which is endothermic ($+0.93 \,\mathrm{eV}$) with a barrier of 2.76 eV. The pathway for reaction (R1), producing WF₅H_(g)/Si-F_(s), is depicted in Fig. 5 as a straight, downward arrow.

Following reaction (R1), WF₅H can further react with a hydrogen-terminated site, as depicted in (R2) and (R2.a), to produce WF₄H₂ (R2) or chemisorbed WF₅ (R2.a):

$$F-Si(100)-H+WF_5H_{(g)}\rightarrow H-Si-F+WF_4H_{2,(g)},$$

$$\Delta E=-0.25\,eV, \eqno(R2)$$

$$\begin{aligned} H - Si(100) - H + WF_5H_{(g)} &\to H - Si - WF_5 + H_{2,(g)}, \\ \Delta E &= -0.19\,\text{eV},\, E_{\ddagger} = 1.56\,\text{eV}. \end{aligned} \tag{R2.a}$$

Reactions (R2) and (R2.a) are both exothermic with calculated energy differences of $-0.25 \, \text{eV}$ (R2) and $-0.19 \, \text{eV}$ (R2.a) with an activation barrier of $1.56 \, \text{eV}$ for reaction (R2.a).

In addition, WF₅H can react similarly with a partially fluorinated site, as depicted in reactions (R3) and (R3.a), to produce WF₄H₂ (R3) or chemisorbed WF₅ (R3.a). However, in this case, Reaction (3) is exothermic $(-0.39 \, \text{eV})$ with a barrier of 2.15 eV, whereas (R3.a) is slightly endothermic $(+0.06 \, \text{eV})$:

$$F - Si(100) - H + WF_5H_{(g)} \rightarrow F - Si - F + WF_4H_{2,(g)},$$

$$\Delta E = -0.39 \text{ eV}, \ E_{\frac{1}{4}} = 2.15 \text{ eV},$$
 (R3)

$$F-Si(100)-H+WF_5H_{(g)}\rightarrow F-Si-WF_5+H_{2,(g)},$$

$$\Delta E=+0.06\,\mathrm{eV}. \eqno(R3.a)$$

The product differences between the above four reactions are illustrated in Figs. 6 and 7.

Comparing the above four reactions between WF₅H and Si(100) [(R2), (R2.a), (R3), and (R3.a)], we see that WF₅H is more likely to undergo ligand exchange at either passivation site to produce WF₄H₂ and is highly unlikely to chemisorb at a partially fluorinated site. Ligand exchange is favored since it results in the formation of an additional surface silicon–fluorine bond, the strongest in the system. Reactions (R2), (R2.a), and (R3) are all thermodynamically probable; however, the activation barrier associated with (R2.a) is lowest, suggesting that, although the production of

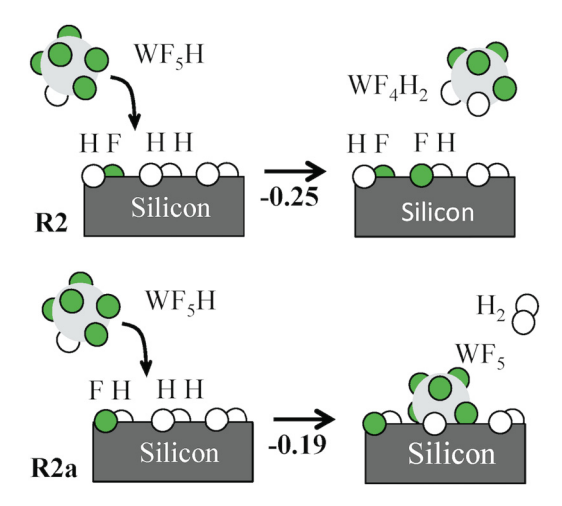
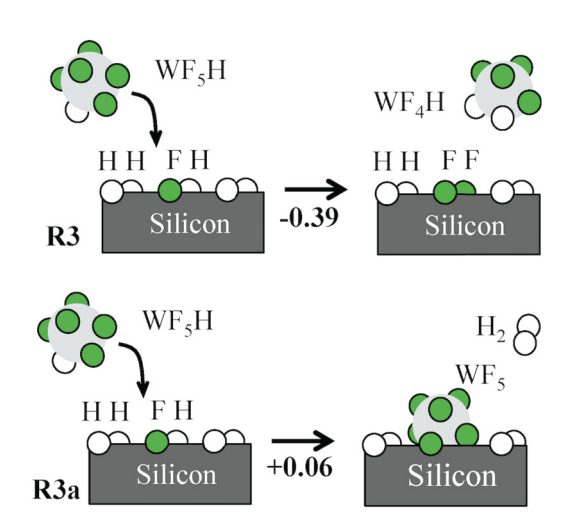


Fig. 6. Illustration of the product differences between multiple reaction pathways for WF_5H on hydrogen-passivated surface sites.



 $F_{\rm IG}$. 7. Illustration of the product differences between the multiple reaction pathways for WF_5H on a partially fluorinated site.

 WF_4H_2 is thermodynamically favored, both products, chemisorbed WF_5 and gaseous WF_4H_2 , will be sampled in the system. A clear difference between (R2), (R2.a), (R3), and (R3.a) is that the adsorption of WF_5 is likely to occur on a surface site containing two hydrogen atoms, whereas WF_4H_2 production is favorable at both sites, with the partially fluorinated site being more favorable. The production of HF is highly unlikely at lower temperatures as supported by (R1.hf) and parallel endothermic reactions using the products from (R1), as shown in (R2.hf) and (R3.hf):

$$H - Si(100) - H + WF_5H_{(g)}$$

 $\rightarrow H - Si(100) - WF_4H + HF_{(g)},$ (R2.hf)
 $\Delta E = +1.64 \,\text{eV},$

$$F - Si(100) - H + WF_5H_{(g)}$$

$$\rightarrow F - Si(100) - WF_4H + HF_{(g)},$$

$$\Delta E = +1.88 \text{ eV}.$$
(R3.hf)

For the pathways leading to gas-phase WF_4H_2 [(R2) and (R3)], WF_4H_2 is unlikely to leave the system as a gas-phase by-product since it strongly physisorbs onto hydrogen-passivated silicon sites with a downhill energy of -1.32 eV. Therefore, consecutive interactions between WF_4H_2 and neighboring hydrogen-passivated silicon sites are likely and may lead to chemisorbed WF_4H (R4) or gas-phase WF_3H_3 (R4.a):

$$\begin{split} H - Si(100) - H + WF_4H_{2,(g)} \\ \rightarrow H - Si(100) - WF_4H + H_{2,(g)}, \\ \Delta E = -0.20 \, \text{eV}, \, E_{\ddagger} = 1.54 \, \text{eV}, \end{split} \tag{R4}$$

$$\begin{split} &H-Si(100)-H+WF_{4}H_{2,(g)}\\ &\to H-Si(100)-F+WF_{3}H_{3}(g),\\ &\Delta E=-0.01\,\text{eV},\,E_{\frac{1}{4}}=2.20\,\text{eV}. \end{split} \tag{R4.a}$$

The production of H_2 and chemisorbed WF₄H (R4) has an overall energy difference of $-0.20\,\text{eV}$ with an activation barrier of 1.63 eV, while the production of gas-phase WF₃H₃ (R4.a) is less favorable with an overall energy difference of -0.01 with an activation barrier of 2.20 eV.

Alternatively, following the divergent pathway involving chemisorbed WF_5 (R2.a) can react successively with a neighboring site to form a silicon–silicon surface dimer. The corresponding reaction mechanism is shown in (R5):

$$\begin{split} & H - Si(100) - H + H - Si(100) - WF_5 \\ & \rightarrow H - Si(100) - Si(100) - WF_5 + H_{2,(g)}, \\ & \Delta E = -0.13 \, \text{eV}, \, E_{\ddagger} = 0.78 \, \text{eV}. \end{split} \tag{R5}$$

The reconstruction of the silicon site with chemisorbed WF₅ to form a surface silicon dimer is thermodynamically downhill (-0.91 eV) with a relatively low barrier (0.79 eV).

In both pathways, surface fluorination through ligand exchange reactions promotes etching of silicon sites since it increases volatility of silicon. For further support, we calculated the complete ligand exchange reaction between molecular WF_6 and SiH_4 . The mechanism for the exothermic reaction is shown below:

$$WF_{6,(g)} + SiH_{4,(g)} \rightarrow SiF_{4,(g)} + WF_2H_{4,(g)},$$

 $\Delta E = -0.2 \text{ eV}.$ (3)

The downhill energy associated with the above reaction indicates that if fluorine is present in the system, silicon will act as a reductant until saturated with fluorine or purged from the reactor. Once silicon surface sites are removed as volatile subfluoride species, a reactive site will be available for W deposition. Therefore, adsorption of WF₆ on Si(100) may proceed through two pathways: (1) at an unetched site to produce volatile H₂ or HF and/or (2) at an etched surface site (Fig. 8). Notably, W deposition is very unlikely to occur at sites containing fluorine, which are favorably produced

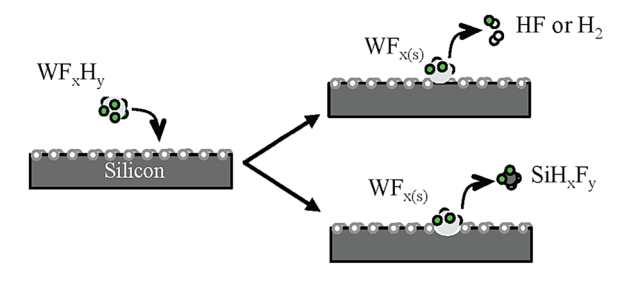


Fig. 8. Adsorption of WF_xH_y on hydrated silicon through an exchange reaction leading to H_2 (or HF) elimination or an etch and deposition step.

according to the above reaction scheme, so these sites are either etched or inactive for the remainder of the ALD process.

B. Reaction of SiH₄ on coalesced, fluorine-terminated W(110)

After nucleation has led to the formation of a fully coalesced tungsten film, SiH₄ is dosed into the system and interacts with deposited W (Fig. 9, bottom half). Crystalline W is therefore used to represent the system surface.

Prior to deposition of WF_6 in succeeding half-cycles on a W(110) surface, SiH_4 plays an essential role of stripping fluorine content from the deposited W surface. The mechanism for SiH_4 reducing fluorine-terminated tungsten [W(110)-F] is shown in (R6), with the reaction path and structures shown in Fig. 10

$$W(110) - F + SiH_{4,(g)}$$

$$\rightarrow W(100) - H_{Bridged} + SiH_3F_{(g)},$$

$$\Delta E = -1.43 \text{ eV}, E_{\dagger} = 0.73 \text{ eV}.$$
(R6)

As depicted in Fig. 9, SiH₄ favorably reacts with W(110)-F to form SiH₃F with a downhill energy of -1.43 eV and an activation barrier of +0.73 eV. The reduction of W(110)-F proceeds until all fluorine content is removed and leads to increased reactivity at reduced sites [W(110)*], which are exposed to gas-phase SiH₄ to form W(110)-SiH_x. The reaction between SiH₄ and reduced W sites to form W(110)-SiH_x is highly exothermic with an energy difference of -3.16 eV. If W(110)* sites and W(110)-F sites are within proximity, SiH₄ favors the removal of fluorine from W(110)-F to chemisorption at W(110)*. In addition, SiH₃F, produced through a reduction reaction between SiH₄ and W(110)-F, can successively interact with the surface and also favors the reduction of W(110)-F to chemisorption at W(110)*. Taking into consideration that SiH_xF_y species are

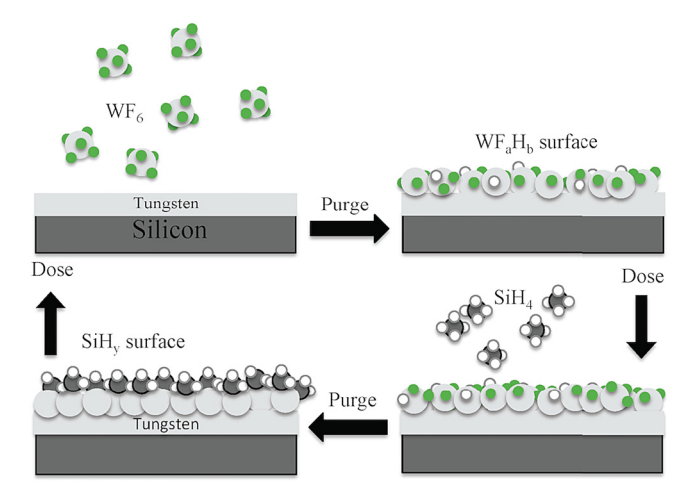


Fig. 9. Schematic of W-ALD after the initial W-ALD cycle: the top half depicts tungsten hexafluoride being exposed to a monolayer of tungsten on a silicon slab and the bottom half depicts silane molecules being exposed to a WFxHy-terminated monolayer of tungsten on a silicon slab.

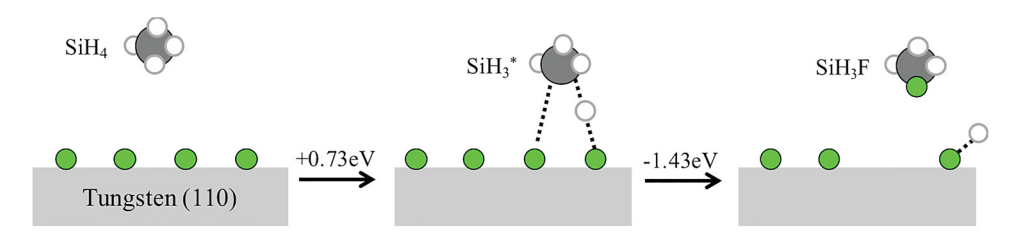


Fig. 10. Reaction energetics and structures for ligand exchange during SiH₄ exposure on fluorine-terminated W(110).

(4)

present in a much lower concentration than SiH_4 , and less likely to chemisorb due to the steric hindrance of fluorine ligands, the predominant chemisorbed species at the end of the cycle is likely SiH_x over SiH_xF_y .

Overall, the reduction of fluorine-terminated W via SiH_4 is supported by the exothermic reaction shown in the mechanism below:

$$4W(110) - F + SiH_{4(g)} \rightarrow 4W(110) * + 2H_2 + SiF_{4,(g)},$$

 $\Delta E = -1.89 \text{ eV}.$

C. Reaction of WF $_6$ on coalesced, SiH $_x$ -terminated W(110)

WF₆ nucleates on W(110)-SiH_x after SiH_x is removed from the surface as gaseous SiH_xF_y (R7). In the mechanism, the stoichiometry of surface species and products are kept indefinite since several reaction pathways exist:

$$WF_{6,(g)} + W(110) - SiH_{x} \to W(110) - WF_{a}H_{b} + SiF_{x}H_{y,(g)}.$$
(R7)

Terminal SiH_x species become volatile as SiH_xF_y through a reduction reaction with gas-phase WF₆ leaving reactive surface sites [W(110)*] available to WF₆ and WF_x exposure. WF_x, a gaseous by-product, is also formed during the surface reduction. WF₆ deposits on W(110)* with an overall energy difference of -3.42 eV through a reaction involving a simultaneous reduction via a neighboring W(110)* site, as depicted in Fig. 11. The formation of W(110)-F leads to the loss of reactivity unless a reductant species (SiH_xF_y) is available to the fluorinated sites. The experimental observation of coalesced films implies that significant W site deactivation must be overcome during deposition or that the depositing

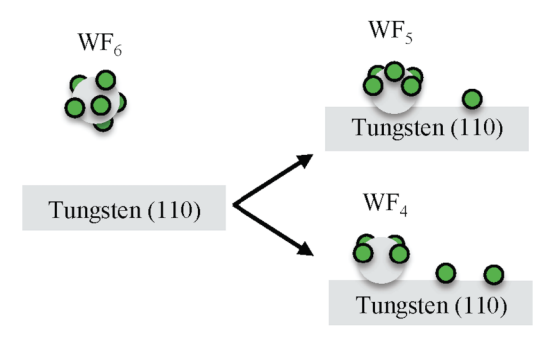


Fig. 11. Illustrations of the interaction between WF₆ and W(110) (R9) to produce chemisorbed tungsten pentafluoride [(R9), $-2.63 \, \text{eV}$] and chemisorbed tungsten tetrafluoride [(R12), $-3.42 \, \text{eV}$].

species is the gaseous by-product, WF_x . Deposition via intermediate WF_x species would lead to less loss of growth sites per W atom. Based on the calculated results, WF_5 and WF_4 are likely by-products that react favorably with $W(110)^*$, with WF_4 being the favored adsorbent. Figure 10 illustrates the loss of reactivity at W(110) sites through WF_6 exposure to form chemisorbed WF_5 and WF_4 .

As previously mentioned, during succeeding SiH₄ doses, if W(110)-F sites are present, SiH₄ will preferentially extract fluorine before silicon deposition proceeds.

IV. DISCUSSION

A. Nucleation of WF₆ on hydrogen-terminated Si(100)

According to the calculated reaction energetics, WF₆ favorably reacts with a silicon surface site to produce hydrogen gas and, at higher temperatures, hydrogen fluoride, which is in agreement with the experimental observation that HF is only observed above 800 K. The typical ALD process is performed at \sim 500 K and, therefore, HF is not considered vital in the ALD process sequence, ^{12,23–25} leaving one predominant elementary reaction step to produce WF₅H (R1). The route leading to chemisorbed WF₅H is significantly favored over the release of HF, allowing us to conclude that tungsten subfluoride vapor products contribute to net W deposition. Furthermore, subfluorides are not detected experimentally using thermal desorption analysis, ²⁴ suggesting that they play a substantial role in the deposition process only as reactive intermediate species.

Prior to the formation of WF₅H, WF₆ physisorbs onto hydrogen-terminated silicon with an energy of $-0.52 \,\mathrm{eV}$; a larger than typical value for physisorption. However, a strong physisorption energy is necessary for the system to overcome the fairly high transition barriers associated with adsorption. These high barriers are supported by the experimental finding that chemisorption of WF₆ is not achieved until the system exceeds 150 K.²⁴ Below this temperature, the energy barrier associated with adsorption (~3 eV) cannot be overcome and interaction is limited to physical adsorption. As the temperature of the system is raised, increased mechanical work and thermal fluctuations contribute to the probability of activation. Once the initial activation barrier is overcome, WF₅H further reacts with surface sites to produce chemisorbed WF₅ or volatile WF₄H₂. The favored production of WF₄H₂ and two terminating fluorine atoms on a single silicon site, along with the exothermic formation of an additional Si-F surface bond, through WF₃H₃ production, supports the formation of volatile SiF_x species. The

formation of SiF_x (x > 1) surface species promotes etching since silicon is stabilized and becomes volatile upon further fluorination. Etching of silicon from the initial Si-H surface is experimentally supported by observed mass loss during the WF₆ dose^{26,27} as well as the experimental detection of SiF_x (x = 0 - 4) above 300 K.²⁴

In addition to surface etching, dimerization of two Si surface atoms is a well-studied phenomenon²⁸ that is energetically feasible during the initial WF₆ dose. This reconstruction would diminish additional reactivity since adsorbed tungsten species would sterically hinder further interaction of adjoined sites. Deactivation of surface sites would support the finding that, at lower cycle numbers (less than five cycles), the mass gain is less than the average for the entire growth period.⁶ Furthermore, it supports the observed delay in conformal tungsten growth on Si(100) at lower cycles.^{29,30} Another factor that may contribute to lower than average mass gain in early cycles is the production of stable Si-F surface bonds which are produced through favorable ligand exchange reactions with WF_xH_y . For deposition to proceed at these sites, the stable Si-F surface species must be etched as SiF_x species, with the predominantly observed species being SiF₄. The removal of the fluorinated surface sites would create additional availability on the Si surface for W deposition; an etch/deposition mechanism that is supported by Elam et al.'s conclusion that during the W-ALD deposition process, a silicon layer of approximately equal thickness to the deposited tungsten layer is consumed.¹⁰ However, etching would become slower as nucleation proceeds since the silicon species would be required to diffuse to the surface before being volatilized.

Based on the energetics and experimental evidence, multiple reaction pathways are occurring simultaneously with the likely by-products being WF_aH_b , SiF_x , and H_2 . For these reaction pathways, WF_6 must encounter at least two surface silicon sites. Since access to two sites would become limited as WF_6 nucleation proceeds, complete W coverage during early doses would require extended precursor dose times.

B. Reaction of SiH_4 on coalesced, fluorine-terminated W(110)

Silane plays the essential, but sacrificial, role of stripping surface fluorine atoms to reduce terminal tungsten groups.⁵ The reduction is highly exothermic [(R7), -1.43 eV] due to the formation of strong Si-F bonds, and H2 and SiF4 make

up the majority of the products evolved. 12,25 As long as fluorine is available on the surface, SiF_xH_y will exchange a hydrogen atom for a fluorine atom before reacting with a bare tungsten site. Once all fluorine content is removed, silane dissociates readily on reduced tungsten sites to hydrogen-terminated $(W_{(s)}-H)$ produce and subhydride-terminated $(W_{(s)}-SiH_x)$ sites. For inadequate exposure of silane, hydrogen-terminated sites will remain at the end of the cycle dose, ^{31,32} while at higher concentrations, H atoms, being the more weakly bound species, will be displaced by silicon subhydrides. Sault and Goodman conclude in their study of silicon-modified W(110) surfaces that the reduction of WF₆ is more favorable when a monolayer of silicon coverage is present on the tungsten surface.²⁵ Therefore, we can conclude that a strong correlation exists between silane pressure and conformality.

C. Reaction of WF $_6$ on coalesced, SiH $_x$ -terminated W(110)

During subsequent dose of WF₆, previously deposited W is passivated by silicon-hydride ($W_{(s)}$ -SiH_x) species. Upon exposure to WF₆, terminal silicon-hydride groups strip fluorine atoms from WF₆ and etch from the surface as volatile SiF_xH_y species.³³ At lower temperatures (less than 600 K), experimental evidence shows that all silicon is stripped from the surface²⁴ and films are fluorine-free. Therefore, we can conclude that etching of the surface, via WF₆ reduction, leaves reactive W sites available for deposition and that there is a simultaneous etching of SiF_x and deposition of W, resulting in a nonequilibrated state of the surface, which is a driving factor in this half-cycle.

If tungsten surface sites are passivated with hydrogen versus silicon subhydrides, as discussed in Sec. IV B, the site will be less reactive since hydrogen is a weaker reductant. For this reason, an adequate exposure of silane is necessary to displace adsorbed hydrogen atoms.³²

D. Self-limiting nature of ALD half-cycles

1. Initial tungsten dose

For a true ALD process, doses of WF₆ and SiH₄ should be inherently self-limiting. During the tungsten dose, the self-limiting nature has been attributed to (1) the formation of a two-dimensional network of chemisorbed tungsten fluorides, which blocks a further reduction of WF₆^{34,35} and (2)

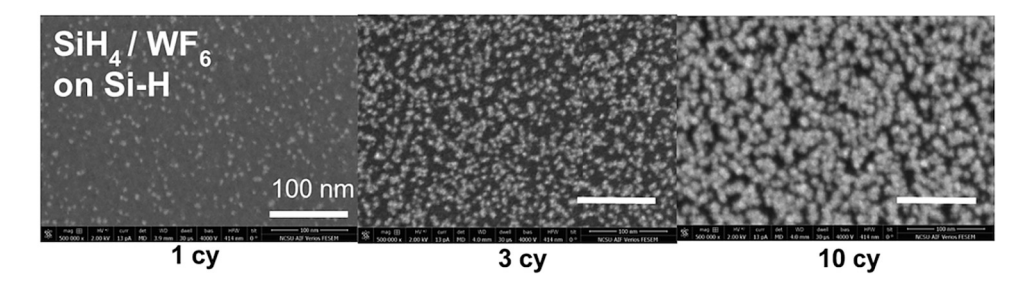


Fig. 12. SEM images of W nuclei on Si(100) after one, three, and ten ALD cycles. Reprinted from P. C. Lemaire, M. J. King, and G. N. Parsons, J. Chem. Phys. **146**, 052811 (2017), with the permission of AIP Publishing.

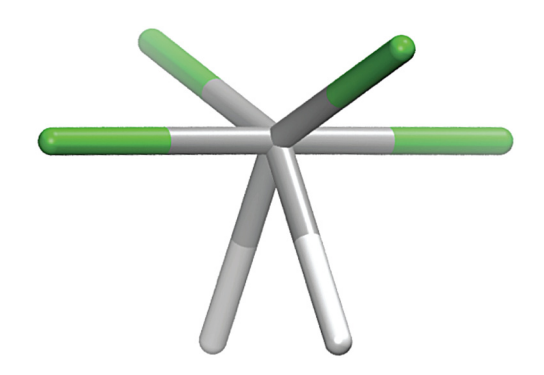


Fig. 13. Illustration of the near-planar conformational arrangement of WF_4H_2 : tungsten (center atom), fluorine (top four atoms) and hydrogen (bottom two atoms).

sealing of the Si substrate from WF₆ by coalesced W. However, the latter explanation does not account for the highly porous films (density of 75% bulk value)²³ and the ability of silicon atoms to penetrate through metallic tungsten. ^{24,36–38} Therefore, the reduction of WF₆ by Si(100) silicon atoms would be possible until the tungsten film was coalesced. The density of the nuclei in the W-ALD film is shown in the SEM image in Fig. 12. ³⁰

Our DFT results support the formation of the two-dimensional network of tungsten sub-fluorides. Specifically, we find that adsorbed tungsten subfluorides undergo a conformational change so that fluorine atoms are close to being on the same plane (Figs. 11 and 13). This planar conformation of fluorine atoms creates a network between neighboring sites and can lead to polymerization into a two-dimensional network on the substrate surface blocking a further reduction of WF₆ by the silicon surface. Deposition in sequential doses is highly dependent on the removal of fluorine ligands by the reductant, in this case, silane. This conclusion is in agreement with the experimental observation that smaller reductant exposures lead to less silicon uptake and therefore less W deposition in successive WF₆ half-cycles.³⁰

As further support, Lifshitz and Green studied similarities between Mo and W deposition on silicon and found that two key differences exist: (1) W deposition had a self-limiting nature, whereas Mo had continuous growth and (2) the fluorine concentration in the W films was an order of magnitude larger than in Mo. From these findings, they suggested that the self-limiting reaction was due to the presence of fluorine-containing intermediates. However, it should be noted that with adequate concentrations of SiH₄, W films will be fluorine-free.³⁵

2. Silane dose

The self-limiting nature of the SiH₄ half-cycle is attributed to silicon-hydride saturation of the W surface following the removal of terminal fluorine as SiF_xH_y . Support for this conclusion is drawn from the experimental finding that as silicon coverage increases on a W(110) surface, the probability of silane dissociation remains greater than 0.5 until a monolayer of silicon is deposited. Once the first monolayer is complete, the probability of silane dissociation decreases

sharply to less than 0.0135. Therefore, the reaction is limited by the availability of tungsten sites, which become inactive after adsorption of silicon-hydrides.

V. SUMMARY AND CONCLUSIONS

In this paper, we present a detailed analysis of reaction mechanisms that lead to nucleation during the deposition process of tungsten on Si(100) and W(110). Results from this study support the experimental observation that when the system is below the ALD temperature "window," the system cannot overcome the energy barriers associated with WF₆ chemisorption and is therefore limited to physical adsorption. Interactions change significantly once the exposure temperature is sufficiently high enough to sample chemisorption pathways. During the WF₆ dose, WF₆ interacts with silicon surface sites with a ratio of 1:2 to produce chemisorbed WF_xH_y. This ratio would result in incomplete coverage on the surface. However, the removal of stable Si- $F_{(s)}$ sites through SiF_xH_y etching creates availability on the surface for additional deposition. Conformal coverage of tungsten during the first dose therefore depends on the etching of fluorine-stabilized silicon sites. However, partial W coverage is supported during the early cycles since adsorbed WF_x species would act as steric inhibitors to etching and deposition as the cycle proceeds. Therefore, until the film has coalesced, the Si(100) surface acts as a reducing agent in the early cycles of WF₆. In the sequential half-cycle, SiH₄ plays the essential role of extracting fluorine atoms from the newly formed W layer. Additional deposition is dependent on the reduction of chemisorbed WF_x since WF₆ cannot adsorb onto WF_x. Once all the fluorine is removed, additional SiH₄ molecules dissociate on bare surface sites to generate a monolayer of silicon-hydrides. The self-limiting nature is attributed to silicon-hydride saturation on the W surface. An inadequate concentration of SiH₄ would result in hydrogen-passivated sites, which would lessen the concentration of SiH_x sites, which act as reducing agents in consecutive doses. Once a conformal film has been deposited, WF₆ interacts with a layer of silicon-hydrides on W(110), which act as the reductants of WF₆ and are removed as volatile SiF_xH_y species. Conversion of surface siliconhydrides to silicon-subfluorides, with WF₆ acting as the fluorine donor, is an essential step for the silicon-hydride monolayer to "etch" from the surface as a volatile, gas-phase species. Thermodynamically favorable removal of this monolayer reinforces the experimental observation that the W-ALD films contain no measurable concentration of fluorine or silicon. The self-limiting nature of later half-cycles of WF₆ is attributed to the complete removal of silicon-hydrides from the surface since these species act as the reductants of WF₆. Based on the energetics and experimental evidence, WF_xH_y, SiF_x, and H2 molecules are released during the ALD process. Strong surface attractions calculated for tungsten subfluorides, e.g., WF₅H and WF₄H₂, support the absence of these species in experimental gas-phase analysis. Conclusions drawn from these data can be extended to study the selective deposition on silicon and silica. 23,30,39,40

By-products that may contribute to nucleation on the nonselective surfaces are WF_aH_b , SiF_xH_v , and H_2 .

ACKNOWLEDGMENTS

The authors acknowledge the financial support from the Semiconductor Research Corporation (Task No. 2401.001) and the National Science Foundation (Award No. 1704151).

- ¹R. Clark, K. Tapily, K.-H. Yu, T. Hakamata, S. Consiglio, D. O'Meara, C. Wajda, J. Smith, and G. Leusink, APL Mater. **6**, 058203 (2018).
- ²Y. Nishi and R. Doering, Handbook of Semiconductor Manufacturing Technology, 2nd ed. (Taylor and Francis Group, Bocan Raton, FL, 2017).
 ³NTRS, The National Technology Roadmap for Semiconductors

(Semiconductor Industry Association, Washington, DC, 2015).

- ⁴V. A. Wells, Materials Research Society, and Workshop on Tungsten and Other Refractory Metals for VLSI Applications, in *Tungsten and Other Refractory Metals for VLSI Applications III* (Materials Research Society, Pittsburgh, PA, 1988).
- ⁵J. W. Klaus, S. J. Ferro, and S. M. George, Thin Solid Films **360**, 145 (2000).
- ⁶F. H. Fabreguette, Z. A. Sechrist, J. W. Elam, and S. M. George, Thin Solid Films 488, 145 (2005).
- ⁷S. E. Atanasov, B. Kalanyan, and G. N. Parsons, J. Vac. Sci. Technol. A **34**, 01A148 (2015).
- ⁸S. M. George, Chem. Rev. **110**, 111 (2010).
- ⁹P. C. Lemaire and G. N. Parsons, Chem. Mater. **29**, 6653 (2017).
- ¹⁰J. Elam, C. Nelson, R. Grubbs, and S. George, Surf. Sci. 479, 121 (2001).
- ¹¹R. K. Grubbs, N. J. Steinmetz, and S. M. George, J. Vac. Sci. Technol. B 22, 1811 (2004).
- ¹²M. L. Yu and B. N. Eldridge, J. Vac. Sci. Technol. A 7, 625 (1989).
- ¹³P. Hohenberg and W. Kohn, Phys. Rev. **136**, B864 (1964).
- ¹⁴W. Liu, A. Tkatchenko, and M. Scheffler, Acc. Chem. Res. 47, 3369 (2014).
- ¹⁵A. S. Sandupatla, K. Alexopoulos, M.-F. Reyniers, and G. B. Marin, J. Phys. Chem. C **119**, 18380 (2015).
- ¹⁶M. Shirazi and S. D. Elliott, J. Comput. Chem. **35**, 244 (2014).
- ¹⁷G. Kresse and J. Furthmuller, Comp. Mater. Sci. 6, 15 (1996).
- ¹⁸G. Kresse and J. Hafner, Phys. Rev. B **49**, 14251 (1994).

- ¹⁹W. E, W. Ren, and E. Vanden-Eijnden, Phys. Rev. B 66, 052301 (2002).
- ²⁰B. Peters, A. Heyden, A. T. Bell, and A. Chakraborty, J. Chem. Phys. 120, 7877 (2004).
- ²¹A. Jain, S. Ong, G. Hautier, W. Chen, W. Richards, S. Dacek, S. Cholia, D. Gunter, D. Skinner, G. Ceder, and K. Persson, APL Mater. 1, 011002 (2013).
- ²²R. Tran, Z. Xu, B. Radhakrishnan, D. Winston, W. Sun, K. A. Persson, and S. P. Ong, Sci. Data 3, 160080 (2016).
- ²³Gokce and Huseyin, Kinetics of the Tungsten Hexafluoride-Silane Reaction for the CVD of Tungsten (Montana State University, 1991).
- ²⁴R. B. Jackman and J. S. Foord, Surf. Sci. 201, 47 (1988).
- ²⁵M. L. Yu, K. Y. Ahn, and R. V. Joshi, IBM J. Res. Dev. **34**, 875 (1990).
- ²⁶J. R. Creighton, Thin Solid Films **241**, 310 (1994).
- ²⁷Y. Xu, Real-Time In-Situ Chemical Sensing, Sensor-Based Film Thickness Metrology, and Process Control in W-CVD Process (A. James Clark School of Engineering, College Park, MD, 2001).
- ²⁸C. S. Guo, W. J. Fan, and R. Q. Zhang, Solid State Commun. 137, 553 (2006).
- ²⁹J. W. Elam, J. A. Libera, M. J. Pellin, A. V. Zinovev, J. P. Greene, and J. A. Nolen, Appl. Phys. Lett. **89**, 053124 (2006).
- ³⁰P. C. Lemaire, M. King, and G. N. Parsons, J. Chem. Phys. **146**, 052811 (2017).
- ³¹A. G. Sault and D. W. S. N. L. Goodman, J. Catal. **126**, 1 (1990).
- ³²A. G. Sault and D. W. Goodman, Surf. Sci. 235, 28 (1990).
- ³³N. Kobayashi, Y. Nakamura, H. Goto, and Y. Homma, J. Appl. Phys. **73**, 4637 (1993)
- ³⁴Heung Lak Park, Chong Do Park, and J. S. Chun, Thin Solid Films 166, 37 (1988).
- ³⁵N. Lifshitz and M. L. Green, J. Electrochem. Soc. **135**, 1832 (1988).
- ³⁶S. V. Plyushcheva, P. G. M. Mikhailov, and A. V. Andreeva, The Investigation of Chemical and Interface Interactions at the Growth of Tungsten Thin Films on Silicon Substrate, Moravian-silesian region, Czech Republic (ZDAS, Ostrava, Czech Republic, 2009).
- ³⁷S. V. Plyushcheva, G. M. Mikhailov, L. G. Shabel'nikov, and S. Y. Shapoval, Inorg. Mater. 45, 140 (2009).
- ³⁸K. Suguro, Y. Nakasaki, T. Inoue, S. Shima, and M. Kashiwagi, Thin Solid Films 166, 1 (1988).
- ³⁹B. Kalanyan, M. D. Losego, C. J. Oldham, and G. N. Parsons, Chem. Vap. Depos. **19**, 161 (2013).
- ⁴⁰B. Kalanyan, P. C. Lemaire, S. E. Atanasov, M. J. Ritz, and G. N. Parsons, Chem. Mater. 28, 117 (2016).